



**HAL**  
open science

## Optical trapping and fast discrimination of label-free bacteriophages at the single virion level

Nicolas Villa, Enrico Tartari, Simon Glicenstein, Hugues de Villiers de la Noue, Emmanuel Picard, Pierre Marcoux, Marc Zelsmann, Grégory Resch, Emmanuel Hadji, Romuald Houdré

► **To cite this version:**

Nicolas Villa, Enrico Tartari, Simon Glicenstein, Hugues de Villiers de la Noue, Emmanuel Picard, et al.. Optical trapping and fast discrimination of label-free bacteriophages at the single virion level. Small, 2024, 10.1002/sml.202308814 . hal-04431362

**HAL Id: hal-04431362**

**<https://hal.science/hal-04431362v1>**

Submitted on 11 Sep 2024

**HAL** is a multi-disciplinary open access archive for the deposit and dissemination of scientific research documents, whether they are published or not. The documents may come from teaching and research institutions in France or abroad, or from public or private research centers.

L'archive ouverte pluridisciplinaire **HAL**, est destinée au dépôt et à la diffusion de documents scientifiques de niveau recherche, publiés ou non, émanant des établissements d'enseignement et de recherche français ou étrangers, des laboratoires publics ou privés.



Distributed under a Creative Commons Attribution - NonCommercial - NoDerivatives 4.0 International License

# Optical Trapping and Fast Discrimination of Label-Free Bacteriophages at the Single Virion Level

Nicolas Villa,\* Enrico Tartari, Simon Glicenstein, Hugues de Villiers de la Noue, Emmanuel Picard, Pierre R. Marcoux, Marc Zelsmann, Grégory Resch, Emmanuel Hadji, and Romuald Houdré

There is a recent resurgence of interest in phage therapy (the therapeutic use of bacterial viruses) as an approach to eliminating difficult-to-treat infections. However, existing approaches for therapeutic phage selection and virulence testing are time-consuming, host-dependent, and facing reproducibility issues. Here, this study presents an innovative approach wherein integrated resonant photonic crystal (PhC) cavities in silicon are used as optical nanotweezers for probing and manipulating single bacteria and single virions with low optical power. This study demonstrates that these nanocavities differentiate between a bacterium and a phage without labeling or specific surface bioreceptors. Furthermore, by tailoring the spatial extent of the resonant optical mode in the low-index medium, phage distinction across phenotypically distinct phage families is demonstrated. The work paves the road to the implementation of optical nanotweezers in phage therapy protocols.

## 1. Introduction

Inappropriate antibiotic use and the lack of drugs acting through novel mechanisms hinder the management of ever-evolving difficult-to-treat infections.<sup>[1–4]</sup> This challenge has been characterized as underpinning an impending major threat to human health.<sup>[5,6]</sup> The therapeutic use of species-specific bacterial viruses called bacteriophages (or phages) represents a promising potential intervention. This approach, termed phage therapy, has been regaining interest lately.<sup>[7]</sup> While many case reports and series support phages as promising adjuvants or alternatives to antibiotics,<sup>[8–13]</sup> recent clinical trials results advocate for the development of individualized approaches to improve outcomes.<sup>[14–17]</sup>

The realization of a personalized approach will require a fast and efficient selection of phages that affect the bacterial strain infecting a particular patient from a phage library that may include >100 different phages.<sup>[18]</sup> Rapid phage susceptibility testing (PST) and phage characterization advancement are essential for achieving the phage selection necessary for implementation of phage therapies.<sup>[19–21]</sup>

Classical PST methods involve diluted drop/spot or turbidity assays. Currently, PST is conducted primarily with phagograms, arrays analogous to antibiograms for antibiotic susceptibility testing.<sup>[22]</sup> Although simple, these methods require 16–24 h of incubation at 37 °C to obtain a readable result and they do not provide information beyond virulence. Although mass spectrometry and flow cytometry techniques have been used in efforts to improve phage characterization efficiency,<sup>[23–25]</sup> their use is constrained by their dependence on pre-labeled phages, costly equipment, and reagents; and they have reproducibility and time limitation issues.<sup>[20,25]</sup> Innovative approaches enabling label-free single-cell studies could help to overcome current obstacles to phage selection.

The field of optical trapping emerged from the pioneering work of Ashkin, who proposed to use light as an optical tweezer to manipulate bacteria and viruses.<sup>[26]</sup> However, free-space optical tweezers are inherently limited due to light diffraction, require bulky and expensive benchtop equipment, and use high-power lasers that risk subjecting viruses to photodamage.<sup>[27,28]</sup> The recent emergence of near-field optics is enabling the engineering

N. Villa, E. Tartari, R. Houdré  
Institut de Physique  
École Polytechnique Fédérale de Lausanne  
Lausanne CH-1015, Switzerland  
E-mail: nicolas.villa@epfl.ch

S. Glicenstein, E. Picard, E. Hadji  
Univ. Grenoble Alpes, CEA, Grenoble INP, IRIG, PHELIQS  
Grenoble 38000, France

H. de Villiers de la Noue, G. Resch  
Laboratory of Bacteriophages and Phage Therapy  
Center for Research and Innovation in Clinical Pharmaceutical Sciences (CRISP)

Lausanne University Hospital (CHUV)  
Lausanne 1011, Switzerland

P. R. Marcoux  
Univ. Grenoble Alpes, CEA, LETI, DTIS, L4IV  
Grenoble 38000, France  
E-mail: pierre.marcoux@cea.fr

M. Zelsmann  
Université Grenoble Alpes, CNRS, CEA/LETI Minatec, LTM  
Grenoble 38000, France

 The ORCID identification number(s) for the author(s) of this article can be found under <https://doi.org/10.1002/smll.202308814>

© 2024 The Authors. Small published by Wiley-VCH GmbH. This is an open access article under the terms of the [Creative Commons Attribution-NonCommercial-NoDerivs](#) License, which permits use and distribution in any medium, provided the original work is properly cited, the use is non-commercial and no modifications or adaptations are made.

DOI: 10.1002/smll.202308814

of nanoscale optical fields that make object manipulation with low optical power possible; such fields can be used for optical tweezing that can be fully exploited at small dimensions.<sup>[29]</sup> Harnessing these advancements, efficient optical traps integrated within dielectric substrates have been used to observe and manipulate microbiological entities.<sup>[30–34]</sup> However, it remains very difficult to retrieve information about the object being trapped, such as its size or morphology, without additional bulky and time-consuming analytical tools.

Here, we report on-chip optical trapping of bacteria and, for the first time, phage trapping and differentiation with 2D hollow resonant dielectric photonic crystal nanocavities. Trapping and sensing are achieved with a lab-on-a-chip (LOC) platform by tailoring the resonant optical mode profile to extend into the low-index medium, thus generating strong electromagnetic field interactions with biological entities. The interactions produced enhance the biological entities resonant-mode perturbation, resulting in unambiguous differentiation between bacteria and phages, as well as among phages from phenotypically distinct families. Silicon transparency in the near-infrared (NIR) spectral range, the hollow nature of optical nanocavities, and the dynamism of light-matter interactions enable manipulation with very low optical power. Our LOC platform allows rapid and reproducible identification of phenotypic properties both at the single-phage or single-bacterium level. On one hand, single-bacterium trapping can yield fast PST necessary for the selection of the most efficient phages. On the other hand, single-phage trapping could provide the fast quantitative determination, prior to administration, of all the different active phages in a given cocktail based on a host-free phenotypic characterization.<sup>[35]</sup> These two types of testing are both based on either previously isolated and identified bacteria suspended in nutritive broth, or on purified therapeutic phages. This means that both tests can be performed in the microfluidic channels of our optofluidic lab-on-a-chip. Therefore, the presented work can contribute effectively to the progress crucially needed for personalized phage therapy.

## 2. Results and Discussion

### 2.1. Lab-on-a-Chip and Sensing Mechanism

As depicted in **Figure 1a**, our LOC is comprised of three layers: a silicon-on-insulator photonic chip with suspended 2D hollow PhC cavities that serve as optical traps; an SU-8 microfluidic circuit layer that enables the transport of biological suspensions; and a glass coverslip that seals the optofluidic chip while allowing for optical imaging. Fluids are injected and collected via inlet and outlet tubes on a polydimethylsiloxane interconnect. The microfluidics can be filled and flushed in a few minutes, e.g.  $\approx 5$  min, which is the response time limiting factor (see Supporting Information Microfluidic circuitry). A tunable laser injects NIR light into the photonic chip via the input fiber. The output fiber collects and sends transmitted light to a photodiode that records its power ( $T$ ) over time. For fabrication technology details, see the Experimental Section.

The PhC membrane is a triangular lattice of holes of radius  $r$  and periodicity  $a$  ( $a = 0.42 \mu\text{m}$ ,  $r/a = 0.262$ ) comprising a W1 access waveguide (**Figure 1b,c**). Several parameters

must be addressed when designing optical resonators for on-chip optical trapping. The resonance wavelength and quality factor are paramount properties of PhC cavities. In particular, a cavity with a very narrow linewidth can be disadvantageous for acquiring relevant information about different objects. Furthermore, one must pay attention to the overlap between the optical field and the low-index medium to design efficient integrated optical tweezers. Increasing the overlap enhances nanoscale light-matter interactions, thus strengthening trapping and analysis performance.

Here, we designed and evaluated two types of PhC cavities (H2 hollow cavity or L3 slot cavity) as shown in the scanning electron microscopy (SEM) images in **Figure 1b,c**. H2 cavities, first employed for biosensing by Fauchet et al.,<sup>[36]</sup> were subsequently used as optical tweezers to demonstrate the self-induced back action (SIBA) mechanism with a dielectric optical resonator and to differentiate the Gram type of bacterial species.<sup>[37,38]</sup> A guided-mode expansion simulation<sup>[39]</sup> of an H2 cavity that supports a resonant mode with part of the optical field overlapping with the central hole is shown in **Figure 1d**; the field maxima are retained in the silicon layer. In parallel, we designed an L3 slot cavity with a resonant optical mode that extends significantly into the low-index medium with an intense lobe at each end of the slot (**Figure 1e**). In our LOC, the H2-cavity central hole has a radius of  $0.35 \mu\text{m}$  and the L3 cavity slot is  $0.66 \mu\text{m}$  long and  $0.16 \mu\text{m}$  wide. According to the spectra normalized to the resonance transmission value, the H2 cavity displays a resonance wavelength of  $\lambda_{\text{res}}^{\text{H}_2} = 1561.9 \text{ nm}$  with a quality factor of  $Q^{\text{H}_2} \approx 3000$ , and the L3 cavity is resonant at  $\lambda_{\text{res}}^{\text{L}_3} = 1565.1 \text{ nm}$  with a quality factor of  $Q^{\text{L}_3} \approx 1300$  (**Figure 1f,g**, respectively). The difference in quality factors between the cavities is due to larger radiation losses for the L3 cavity arising from the low-index location of its resonant mode. The optical power coupled to both cavities in resonance is estimated to be in the range of  $0.7\text{--}1.0 \text{ mW}$ , after accounting for insertion/propagation losses and the evanescent coupling efficiency between the W1 waveguide and the cavity.

When the laser wavelength is tuned to match a cavity's resonance, evanescent coupling with the W1 waveguide excites the corresponding resonant optical mode, thereby activating the optical trap. A representative example of a normalized transmission measurement of a bacterium trapped in an H2 hollow PhC cavity is shown in **Figure 1h**. Briefly, the optical output power recording for each trial starts while the tunable laser is off, thus producing a zero transmitted value (OFF, black). A few seconds later, the tunable laser is switched on, exciting the optical mode at resonance ( $\lambda_{\text{exc}} = \lambda_{\text{res}}$ ). The corresponding transmitted power then proceeds to increase up to the empty cavity resonance level (ON, green).

The optical mode is then perturbed as soon as an object gets trapped, causing the transmission to increase to a greater value  $T_{\text{shift}}$  (TRAPPING, red). The inset in **Figure 1h** presents the cavity's spectral characteristics when empty (green spectra) and when full (red spectra) with the unnormalized transmission values  $T_{\text{full}}$  and  $T_{\text{empty}}$  defined such that  $T_{\text{shift}} = T_{\text{full}}/T_{\text{empty}}$ . We normalize the transmission to the empty cavity resonance level to facilitate comparisons. This procedure does not change the signal interpretation as the quality factor of the cavity does not

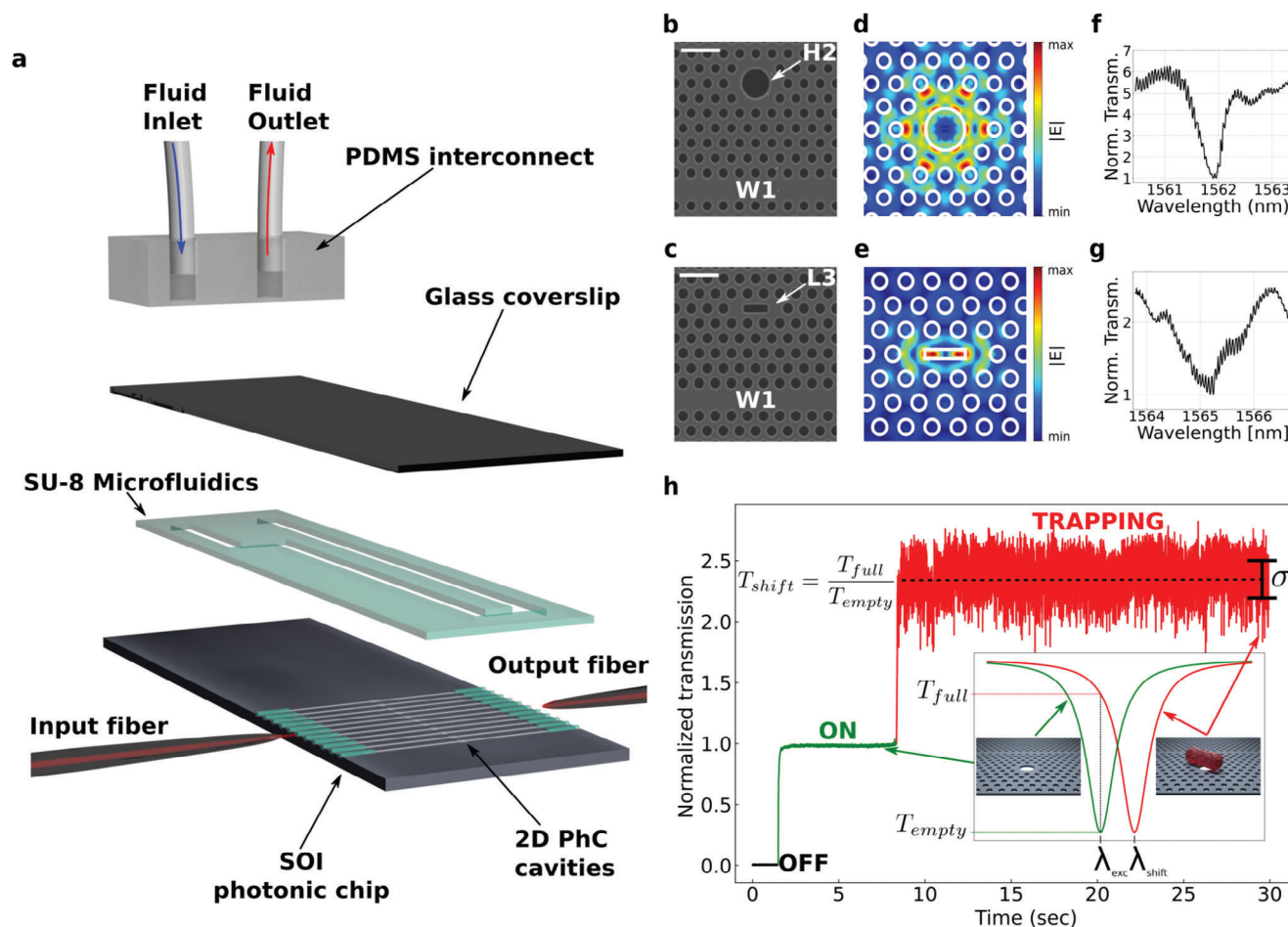


**Figure 1.** Optofluidic sample, end-fire setup, PhC cavity properties, and sensing mechanism. a) Expanded view of optofluidic chip. b, c) SEM of the H2 hollow and the L3 slot cavity revealing the evanescent coupling scheme with a W1 waveguide and their configurations. Scale bar, 1  $\mu\text{m}$ . d, e) GME-simulated resonant-mode profiles corresponding to the cavities. f, g) measured spectra for each cavity normalized to the respective resonance transmission values. h) Normalized transmission measurement of a bacterium trapped in the H2 cavity (cavity OFF, black; cavity ON, green; TRAPPING, red). The normalized transmission most probable value  $T_{\text{shift}}$  and its fluctuations  $\sigma$  were used to characterize the trapping event. Insets show cavity spectra when the trap is empty (green) or filled (red).

significantly vary upon trapping. When on, the resonant field intensity exerts a force on any polarizable object close enough to the cavity to be affected. However, the object's proximity to the cavity perturbs the optical mode, resulting in a shifted spectrum centered at  $\lambda_{\text{shift}}$  and a decrease in cavity energy. Thus, the object tends to escape, but this freedom self-restores a pulling force towards the trap via the SIBA mechanism. This phenomenon retains the object with minimal light intensity and explains the observed fluctuations of normalized transmission that are produced by the residual movement of the trapped object (Figure 1H).<sup>[37,40,41]</sup> Note that given the amount of light coupled to the nanocavities, convective and thermophoretic effects are negligible during the trapping events.

Because optical gradient forces scale with the third power of the object typical dimension, the transmission shift and fluctuation amplitudes ( $\sigma$ ) are object- and cavity-dependent. These characteristics, which depend mainly on the object's refractive index and overlap with the resonant optical field, provide the sensing mechanism of our LOC.<sup>[42,43]</sup> The presented side-coupled exci-

tation scheme and the hollow nature of the cavities provide the characteristics needed to trap and sense microscopic biological entities with different phenotypic properties without any surface bioreceptors or labeling. We must emphasize that we aim to monitor the response of single biological entities over a short time scale (i.e., seconds) rather than monitoring a continuous quantity over several minutes typically presented in detection assays<sup>[44]</sup>. Since our platform has no selectivity, its sensitivity is object-dependent and directly related to the shift in transmission upon trapping. Finally, our approach is intended to work with isolated and identified bacteria or phages in sufficiently high concentrations (Experimental Section).

## 2.2. Single Phage Trapping and Differentiation from a Single Bacterium

Researchers who have taken up the challenge of on-chip optical trapping have found that the relatively large size of

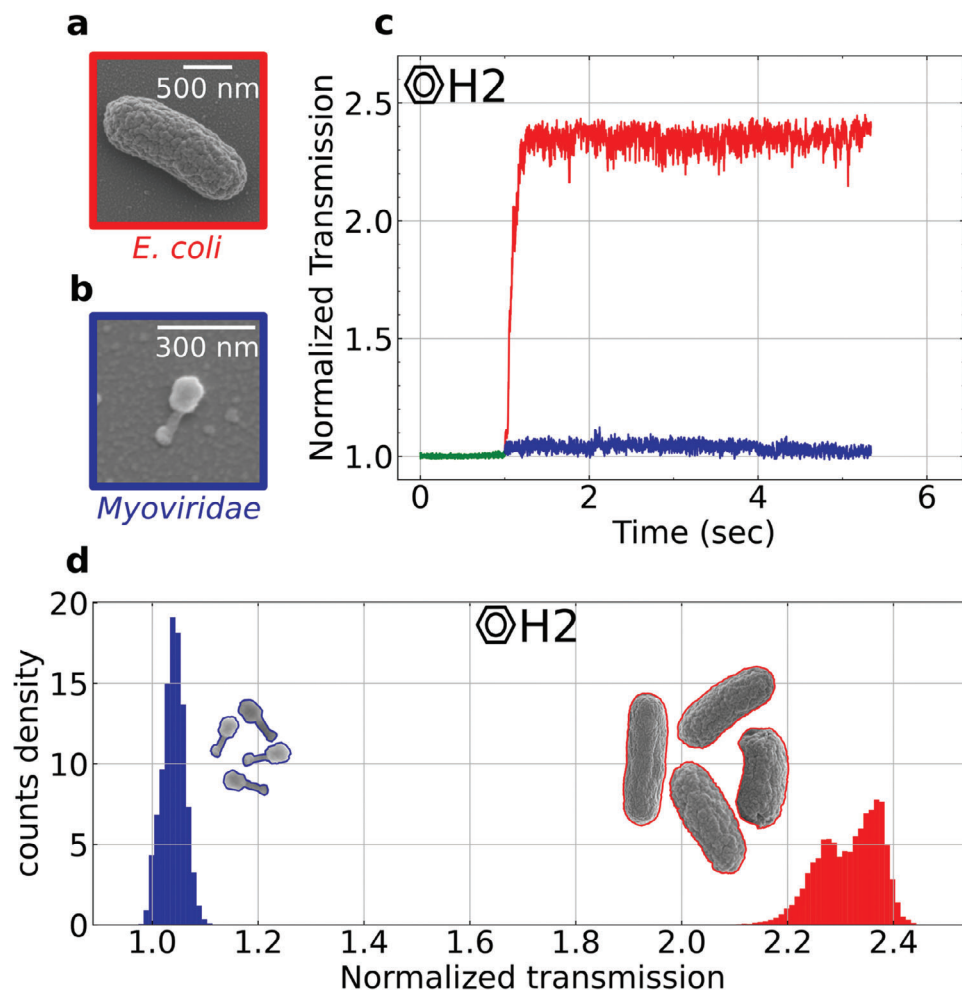


**Figure 2.** Comparison of transmission properties upon bacterium or phage optical trapping with the H2 hollow PhC cavity. a,b) SEM micrographs of *E. coli* strain ATCC 8739 and phage 1042, respectively. c) Normalized time series showing shifts induced by a single phage 1042 (blue) and a single *E. coli* strain ATCC 8739 bacterium (red) on an H2 hollow nanocavity. d) Histograms of multiple single bacteriophage (blue,  $n = 16$ ) and single bacterium (red,  $n = 9$ ) trapping events with the H2 hollow cavity.

bacteria makes them easier to trap than smaller nanoscale biological objects,<sup>[31,38,45,46]</sup> such as viruses, virus-like particles, and vesicles. The fundamental dependence of optical forces on an object's dimensions, polarizability, and field intensity gradient complicates nanoscale-object manipulation.<sup>[47]</sup> Taking advantage of subwavelength variations of the resonant optical field, we aimed to achieve optical trapping of a single bacterium and a single phage in a 2D dielectric hollow PhC cavity. Representative examples of the normalized transmission signal recordings obtained during independent H2-hollow-cavity trapping experiments with a suspension of *Escherichia coli* strain ATCC 8739 (ATCC 8739, Figure 2a) and of *Myoviridae* phage vB\_EcoM\_1042 (1042, Figure 2b) are depicted in Figure 2c (red and blue curve, respectively). The two curves are synchronized to facilitate comparison such that the trapping perturbation of the resonant mode occurs after 1 s in the time series. Detailed information about the experimental conditions is given in the Experimental Section.

In a control experiment, no trapping events were recorded when a sonicated and filtered bacterial suspension was injected into the chip (Figure S2, Supporting information). A distinction

between a trapped bacterium and a trapped phage can be established unambiguously from the relative change in the normalized transmission that is 35 times larger for an *E. coli* bacterium (135%) than for a *Myoviridae* phage (3.8%) (Figure 2c). A second discriminative feature is the amplitude of the fluctuations caused by the trapped entity's residual movement in the trap, which we confirmed to be smaller for the phage ( $\sigma = 0.019$ ) than for the bacterium ( $\sigma = 0.038$ ). The normalized transmission shift of a bacteria is more than two orders of magnitude larger than the variations of the signal before trapping ( $\sigma_{\text{noise}} = 0.005$ ). For the *Myoviridae* phage, the sensitivity is reduced but still one order of magnitude larger than  $\sigma_{\text{noise}}$  ( $(1.038 - 1)/0.005$ ).

Given that viruses and bacteria display similar refractive indices (range, 1.35–1.5),<sup>[24,27,48–50]</sup> the observed resonance shift between a bacterium and a virus can be attributed to the spatial overlap of each entity with the optical mode. Because bacteria are substantially larger than phages, they have greater overlap with the optical cavity mode, leading to a larger shift. Meanwhile, the cavity line shape displays a small derivative close to the resonance (Figure 1f). Hence a small spectrum perturbation leads

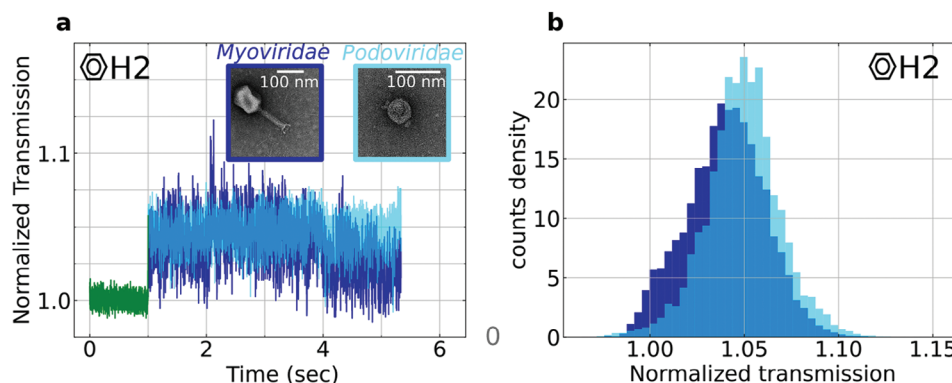


**Figure 3.** Comparison of transmission properties upon *Myoviridae* (blue) and *Podoviridae* (light blue) optical trapping on an H2 hollow cavity. a) Normalized time series showing the shift induced by a single phage 1042 and a single phage gh-1 on an H2 hollow cavity. Insets show transmission electron micrographs of each bacteriophage. b) Histograms of multiple single phage 1042 (blue,  $n = 16$ ) and gh-1 (light blue,  $n = 7$ ) trapping events with the H2 hollow cavity.

comparatively to smaller transmission fluctuations. In contrast, a larger wavelength shift when  $T_{\text{full}}$  is located in the steeper part of the spectrum results in larger fluctuations, see inset Figure 1h. The fact that the fluctuations do not diminish to the level of the empty cavity indicates that the SIBA mechanism is powerful enough to prevent the bacterium from ever escaping from the trap. The relatively tiny size of a phage causes only a slight wavelength shift and reduces the force exerted by the trap, resulting in smaller fluctuations.

Well-separated and independent distributions were obtained from 16 independent *Myoviridae* trapping measurements (normalized transmission =  $1.039 \pm 0.021$ ) and nine *E. coli* bacteria measurements (normalized transmission =  $2.316 \pm 0.057$ , Figure 2d). Interestingly, the distribution dispersion was lower for phages than for bacteria. This observation agrees with the distribution dispersion's relations to variation in object morphology and the different positions the object can take in the trap. Consequently, because of the substantial overlap of a bacterium with the optical field, changes in bacterial shape, size, or positioning can induce sizable shift variations. Conversely, differences in the phenotype or positioning of phages induce only small changes in overlap and thus only slight variations in transmission shift.

In the present experiments, we were able to take advantage of subwavelength variations in the resonant optical field to demonstrate optical trapping of a single bacterium and, for the first time, of a single bacteriophage on a 2D dielectric hollow PhC cavity. When optically trapping bacteriophages, we eventually observed discrete incrementations of the transmission signal. We attribute this stepwise behavior of the signal to the successive trapping of additional phage particles, with the minimal step corresponding to the trapping of one single phage (Figure S3, Supporting information).

### 2.3. Phage Differentiation at the Family Level

*Podoviridae* gh-1 viruses could also be optically trapped in our H2 nanocavity, demonstrating the possibility of using this nanocavity to trap phages from different families. However, the signals obtained from a trapped gh-1 and from a trapped 1042 (*Myoviridae*)

were not readily distinguishable (Figure 3a) and the normalized transmission shift distribution observed for phage 1042 ( $1.039 \pm 0.021$ ) largely overlapped that for the phage gh-1 ( $1.048 \pm 0.019$ , Figure 3b). Although these two phages belong to phenotypically distinct families, their interaction with the trap appears to be too weak to cause distinguishable changes in transmitted power. Of note, we only observed micro-trapping events with the *Ackermanviridae* phage 5008 in the H2 nanocavity (Figure S4, Supporting information).

We tested whether the L3 slot cavity could be used to differentiate between phages. The L3 slot width is comparable to the size of a bacteriophage (Figure S5, Supporting information) and, more importantly, its resonant optical mode profile displays two maxima at the poles of the hollow region. We expected this feature to be an advantage in the manipulation of nanoscopic objects for which optical power must be higher due to the gradient force's dependence on object volume. As a result of these characteristics, phages are likely to be trapped within the slot where light-matter interactions are maximized. A bacterium is too large to enter the slot, and thus induces a lower transmission shift in the L3 nanocavity mode, leading to a normalized transmission signal at  $1.391 \pm 0.043$  (Figure S6, Supporting information), compared to  $2.357 \pm 0.038$  for the H2 nanocavity (Figure 2c).

We compared optical trapping measurements obtained for *Myoviridae* phage 1042 with an H2 hollow cavity versus with an L3 slot nanocavity. We observed that the transmission shift for the L3 slot cavity ( $1.131 \pm 0.014$ , purple, Figure 4a) was approximately 10% larger than for the H2 cavity ( $1.041 \pm 0.018$ , blue, Figure 4a). This result is counter-intuitive given that the quality factor of the H2 nanocavity ( $Q^{H_2} \approx 3000$ ) is higher than that of the L3 nanocavity ( $Q^{L_3} \approx 1300$ ). Indeed, without accounting for the overlap between the trapped object and the optical field, one would expect only a minor transmission shift for a cavity with a lower quality factor for a given spectrum perturbation. The observed results suggest that phage 1042 may perturb the L3 slot resonant mode more than the H2 hollow cavity resonant mode. To investigate this possibility, we performed finite-difference time-domain simulations to compute resonance wavelength shifts upon placing single nanospheres of varying dimensions onto the hollow region of each cavity where the

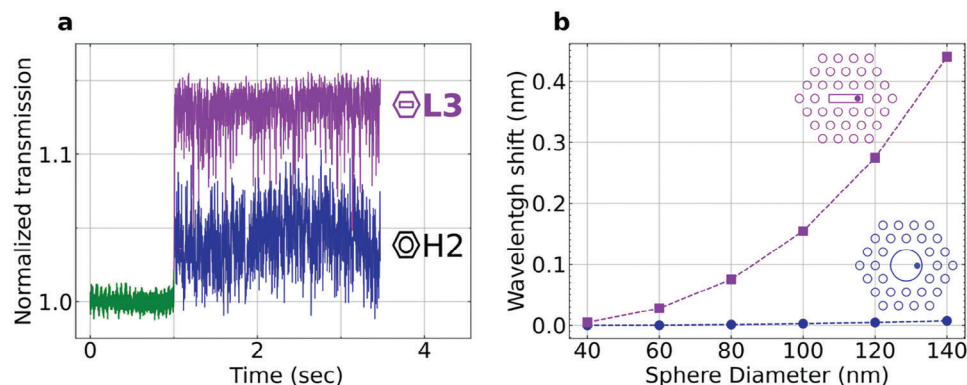


**Figure 4.** Transmission properties upon *Myoviridae* optical trapping with the H2 hollow cavity (blue) versus with the L3 slot cavity (purple). a) Normalized time series showing the shift induced by a single phage 1042 on the H2 hollow cavity (blue) and on the L3 slot cavity (purple). b) Dependence of finite difference time domain simulations of the wavelength shift on size of a nanosphere (refractive index, 1.42) placed in a region of high optical field intensity. Insets show the geometric configuration of simulations for each cavity.

electromagnetic field is high (Figure 4b); the insets in Figure 4b show the schematic configuration of the simulations for both cavities. We set the refractive index of the nanosphere to a typical value of 1.42.<sup>[27]</sup> As observed, the L3 nanocavity has a higher sensitivity for objects in the range of 40–140 nm, which corresponds to the size of the phages under study and confirms our hypothesis.

The L3 slot nanocavity was used to trap phages from three families (*Myoviridae*, *Podoviridae*, and *Ackermannviridae*) with low optical power (Figure 5). Time series data (Figure 5a) show that their interaction with the trap is strong enough for their phenotypical differences to cause changes in transmitted power that are sufficiently distinct to enable their differentiation. In contrast to the H2 nanocavity, the normalized transmission shift histograms obtained from multiple measurements on the L3 slot nanocavity with *Myoviridae* ( $n = 10$ ;  $1.125 \pm 0.017$ ), *Podoviridae* ( $n = 9$ ;  $1.091 \pm 0.024$ ), and *Ackermannviridae* ( $n = 9$ ;  $1.048 \pm 0.017$ ) are separated by distinguishable gaps (Figure e), indicating that each phage family tested perturbs the L3 nanocavity resonant mode differently. Morphologically, the *Myoviridae* (Figure 5b) is very similar to the *Ackermannviridae* (Figure 5d). They are both tailed phages with differences in the capsid geometry, tail length, and fibers. However, their responses (Figure 5a,e) are far from each other. In contrast, The *Podoviridae* (Figure 5d) is morphologically different (no tail) from both phages but shares more similarities regarding their optical signature as its transmitted signal lies between the *Myoviridae* and the *Ackermannviridae* signal. Several characteristics can explain this observation. First, one can hypothesize differences in the structure of the proteins forming each phage. The high sensitivity of the nanoresonators is such that a slight difference in composition, thus in the refractive index, could be responsible for such observations (Figure S7a, Supporting information). Secondly, phages are charged particles, and we should not omit the possibility of electrostatic interactions between the silicon surface and the virion. In this case, the virion might be pulled or pushed away from the center of the photonic crystal slab. If repulsion occurs, it would induce a minor perturbation of the resonant mode due to a smaller overlap with the optical field (Figure S7b, Supporting information). It could also be a joint conse-

quence of both effects. Finally, because we do not see the phages optically, we should consider the eventuality of trapping phage dimers. Despite the overlapping distributions, preventing undeniable discrimination of the three phages, the L3 slot cavity is better suited to study phages at the single particle level than the H2 nanocavity. This result shows that a specific design of an integrated nanotweezer leverages its potential for biosensing applications.

### 3. Conclusion

We demonstrated label-free single-virion optical trapping in dielectric resonant 2D hollow PhC nanocavities and distinction among them from their optical fingerprints in the transmission signal. A new approach was developed by engineering the pattern of the evanescent field in interaction with biological objects. It is based on an L3 slot nanocavity with a resonant mode profile that extends into the low-index medium. The L3 nanocavity was found to be superior to the H2 nanocavity for the differentiation of phages at the family level.

This work has relevant applications in basic phage research and phage therapy. The small dimensions, fast response time, and high sensitivity of our optofluidic device are well-suited to improve on current time-consuming and empiric microbiological tests working with isolated and known organisms. For instance, PST, a critical assay for phage therapy development, is in need of optimization for obtaining faster and more accurate selection of phages to be administered to patients in therapeutic dead-ends due to difficult-to-treat infections.<sup>[51,52]</sup> Additionally, the capacity to distinguish phages at the family level could inform the design and quality control testing of universal and tailored phage cocktails. Indeed, it has been shown previously that mixing phages from different families (*Myoviridae* and *Podoviridae*) was an efficient way to optimize the efficacy of anti-*Staphylococcus aureus* phage cocktails.<sup>[53]</sup> Hence, this work has the potential to make a significant contribution to the essential advancement required for personalized phage therapy.

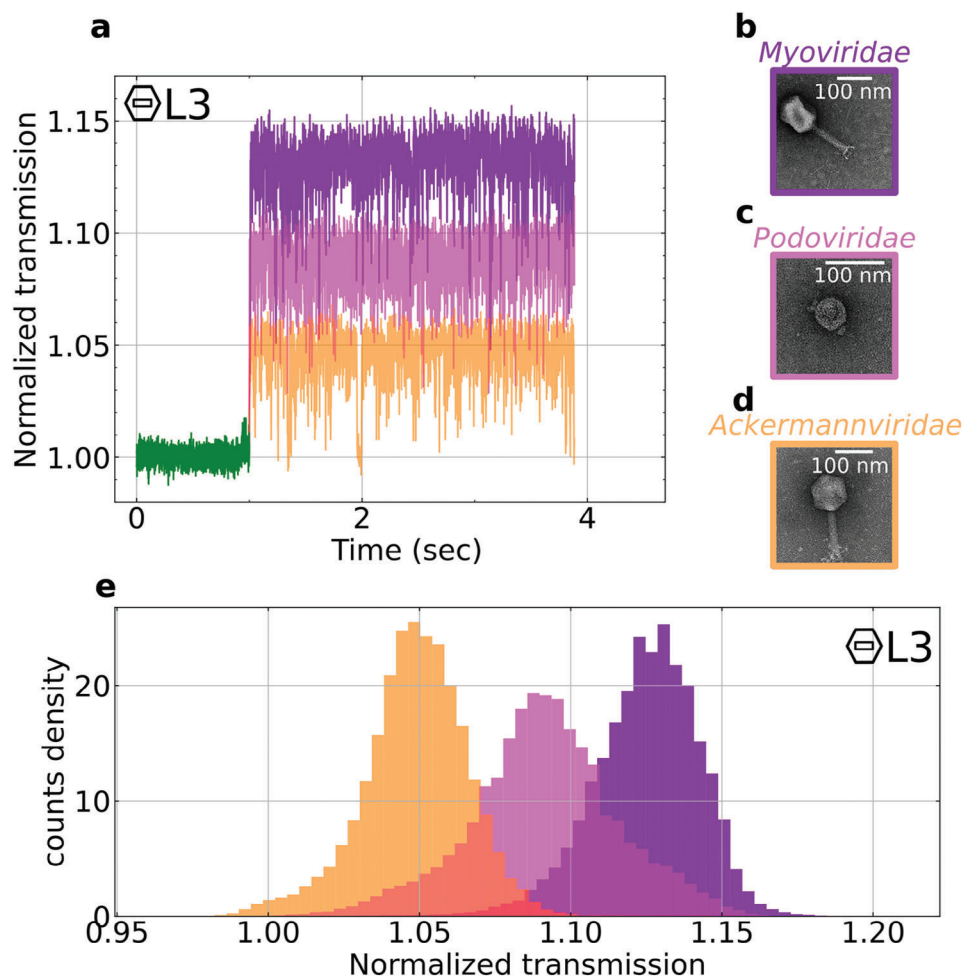


**Figure 5.** Comparison of transmission properties upon *Myoviridae*, *Podoviridae*, and *Ackermannviridae* optical trapping on the L3 slot cavity. a) Normalized time series showing the shift induced by a single phage 1042 (purple), gh-1 (pink), and 5008 on the L3 slot cavity. b–d) Transmission electron micrographs of phage 1042, gh-1, and 5008, respectively. e) Histograms of multiple single phage 1942 (purple,  $n = 10$ ), gh-1 (pink,  $n = 9$ ), and 5008 (orange,  $n = 9$ ) trapping events with the L3 slot cavity.

## 4. Experimental Section

**Optofluidic Chip Fabrication:** The optofluidic chip was manufactured in EPFL cleanrooms. The photonic components were patterned via electron beam lithography on ZEP resist and then transferred to a 220-nm silicon working layer by inductively coupled plasma etching. SU-8 mode converters were then incorporated to increase fiber-waveguide coupling efficiency. A robust and versatile microfluidic process similar to Jackman's process<sup>[54]</sup> was developed (Figure S1, Supporting information). SU-8 microfluidic channels (750  $\mu\text{m}$  wide and 25  $\mu\text{m}$  thick) were patterned by photolithography. After cleavage of the facets, the PhC membrane was released with wet buffered HF etching to ensure good vertical confinement of the optical mode. Finally, a standard glass coverslip for immersion oil microscopy was used to seal the fluidic system. Injection to and collection from the microfluidic circuitry was performed via a polydimethylsiloxane interconnect.

**Bacteria Strain and Phages:** Trapping experiments with *E. coli* strain ATCC 8739 bacteria (Microbiologics, Saint Cloud, MN) and three phages: *E. coli Myoviridae* phage vB\_EcoM\_1042 (1042), *Pseudomonas putida Podoviridae* phage gh-1 (gh-1), and *Klebsiella pneumoniae Ackermannviridae* phage vB\_KpnA\_5008 (5008) were performed (Figure S4, Supporting information). Bacteria were grown on lysogeny broth (LB) agar Petri dishes at 37  $^{\circ}\text{C}$  overnight. Prior to injection, isolated bacterial colonies

were inoculated in a 50% liquid LB, 49.5% deionized water, and 0.5% Triton X-100 solution (v/v). This buffer was used to prevent bacteria from sticking to the silicon surface, as observed with a pure LB medium. After inoculation, bacterial suspensions were vortexed to obtain turbidity in the range of 0.5–1.0 McF. Measurements commenced  $\geq 5$  min after suspension injection into the optofluidic chip. Phage 1042, phage gh-1, and phage 5008 were amplified in *E. coli* strain B (own collection), *P. putida* strain ATCC 12633 (Microbiologics, Saint Cloud, MN), and *K. pneumoniae* strain S155 OXA-48, respectively (Figure S8, Supporting information). Before trapping, phage suspensions were filtered with a polyethersulfone filter (pore size, 0.45  $\mu\text{m}$ ) to remove bacterial residues. Drop dilution testing of the phage suspensions indicated that phage concentrations in the range of  $10^8$ – $10^9$  PFU  $\text{mL}^{-1}$  were obtained. Phages were resuspended in 50% liquid LB, 49.5% deionized water, and 0.5% Triton X-100 solution before being injected into microfluidic channels, resulting in concentrations of  $5 \times 10^7$ – $10^8$  PFU  $\text{mL}^{-1}$ .

**Experimental Procedure:** Samples were injected into chip microchannels through the inlet tube with an external pump. Closing a valve in the fluidic output tubing brings the biological entities into unconstrained Brownian motion. An oil-immersion objective was used for high-resolution optical imaging of trapping events. The optofluidic samples have strong mechanical stability that was sufficiently robust to allow usage for more than 1 year without diminished performance.

## Supporting Information

Supporting Information is available from the Wiley Online Library or from the author.

## Acknowledgements

The authors thank D. Demurtas from the Interdisciplinary Centre for Electron Microscopy (CIME) of EPFL for the transmission electron micrographs of phages. The authors also thank F. Bobard from CIME for her help and discussions concerning the optimization of SEM images. The authors acknowledge M. Croisier from the Bioelectron Microscopy Core facility of EPFL for the preparation of microorganisms for SEM imaging. The authors were grateful to Patrice Nordmann for the kind provision of strain S155 OXA-48. The *Félix d'Hérelle Reference Center for Bacterial Viruses* at the Université Laval (Québec, Canada) was gratefully acknowledged for providing bacteriophage gh-1, as well as bacterial host strain *Pseudomonas putida* ATCC 12633. This work was supported by the Swiss National Science Foundation through grants (no. 310030L\_212772 and no. 200020\_188649), the French RENATECH network and by the French National Research Agency FANR through the grant (no. ANR-22-CE93-0011-01).

Open access funding provided by Ecole Polytechnique Federale de Lausanne.

## Conflict of Interest

The authors declare no conflict of interest.

## Data Availability Statement

The data that support the findings of this study are available from the corresponding author upon reasonable request.

## Keywords

bacteria, bacteriophages, biosensing, microfluidics, optical resonators, optical trapping, photonic crystals

Received: October 3, 2023

Revised: December 13, 2023

Published online: January 28, 2024

- [1] K. Lewis, *Cell* **2020**, *181*, 29.
- [2] E. Tacconelli, E. Carrara, A. Savoldi, S. Harbarth, M. Mendelson, D. L. Monnet, C. Pulcini, G. Kahlmeter, J. Kluytmans, Y. Carmeli, M. Ouellette, K. Outterson, J. Patel, M. Cavalieri, E. M. Cox, C. R. Houchens, M. L. Grayson, P. Hansen, N. Singh, U. Theuretzbacher, N. Magrini, A. O. Aboderin, S. S. Al-Abri, N. Awang Jalil, N. Benzonana, S. Bhattacharya, A. J. Brink, F. R. Burkert, O. Cars, G. Cornaglia, et al., *Lancet Infect. Dis.* **2018**, *18*, 318.
- [3] C. L. Ventola, *Pharm. Ther.* **2015**, *40*, 277.
- [4] B. Aslam, W. Wang, M. I. Arshad, M. Khurshid, S. Muzammil, M. H. Rasool, M. A. Nisar, R. F. Alvi, M. A. Aslam, M. U. Qamar, M. K. F. Salamat, Z. Baloch, *Infect Drug Resist.* **2018**, *11*, 1645.
- [5] C. J. L. Murray, K. S. Ikuta, F. Sharara, L. Swetschinski, G. Robles Aguilar, A. Gray, C. Han, C. Bisignano, P. Rao, E. Wool, S. C. Johnson, A. J. Browne, M. G. Chipeta, F. Fell, S. Hackett, G. Haines-Woodhouse, B. H. Kashef Hamadani, E. A. P. Kumaran, B. McManigal, S. Achalapong, R. Agarwal, S. Akech, S. Albertson, J. Amuasi, J. Andrews, A. Aravkin, E. Ashley, F.-X. Babin, F. Bailey, S. Baker, et al., *The Lancet* **2022**, *399*, 629.
- [6] O'Neill, *Rev. on Anti. Resis.* **2016**.
- [7] J.-P. Pirnay, T. Ferry, G. Resch, *FEMS Microbiol. Rev.* **2022**, *46*, fuab040.
- [8] T. Ferry, C. Kolenda, F. Laurent, G. Leboucher, M. Merabishvili, S. Djebara, C.-A. Gustave, T. Perpoint, C. Barrey, J.-P. Pirnay, G. Resch, *Nat. Commun.* **2022**, *13*, 4239.
- [9] S. Jennes, M. Merabishvili, P. Soentjens, K. W. Pang, T. Rose, E. Keersebilck, O. Soete, P.-M. François, S. Teodorescu, G. Verween, G. Verbeken, D. De Vos, J.-P. Pirnay, *Crit. Care* **2017**, *21*, 129.
- [10] R. M. Dedrick, C. A. Guerrero-Bustamante, R. A. Garland, D. A. Russell, K. Ford, K. Harris, K. C. Gilmour, J. Soothill, D. Jacobs-Sera, R. T. Schooley, G. F. Hatfull, H. Spencer, *Nat. Med.* **2019**, *25*, 730.
- [11] S. Maddocks, A. P. Fabijan, J. Ho, R. C. Y. Lin, N. L. Ben Zakour, C. Dugan, I. Kliman, S. Branston, S. Morales, J. R. Iredell, *Am. J. Respir. Crit. Care Med.* **2019**, *200*, 1179.
- [12] E. J. Cano, K. M. Caflisch, P. L. Bollyky, J. D. Van Belleghem, R. Patel, J. Fackler, M. J. Brownstein, B. Horne, B. Biswas, M. Henry, F. Malagon, D. G. Lewallen, G. A. Suh, *Clin. Infect. Dis.* **2021**, *73*, e144.
- [13] S. Aslam, E. Lampley, D. Wooten, M. Karris, C. Benson, S. Strathdee, R. T. Schooley, *Open Forum Infect. Dis.* **2020**, *7*, ofaa389.
- [14] P. Jault, T. Leclerc, S. Jennes, J. P. Pirnay, Y.-A. Que, G. Resch, A. F. Rousseau, F. Ravat, H. Carsin, R. L. Floch, J. V. Schaal, C. Soler, C. Fevre, I. Arnaud, L. Bretraudeau, J. Gabard, *Lancet Infect. Dis.* **2019**, *19*, 35.
- [15] S. A. Sarker, S. Sultana, G. Reuteler, D. Moine, P. Descombes, F. Charton, G. Bourdin, S. McCallin, C. Ngom-Bru, T. Neville, M. Akter, S. Huq, F. Qadri, K. Talukdar, M. Kassam, M. Delley, C. Loiseau, Y. Deng, S. El Aidi, B. Berger, H. Brüssow, *EBioMedicine* **2016**, *4*, 124.
- [16] L. Leitner, W. Sybesma, N. Chanishvili, M. Goderdzishvili, A. Chkhotua, A. Ujmajuridze, M. P. Schneider, A. Sartori, U. Mehnert, L. M. Bachmann, T. M. Kessler, *BMC Urol.* **2017**, *17*, 90.
- [17] J.-P. Pirnay, E. Kutter, *Lancet Infect. Dis.* **2021**, *21*, 309.
- [18] T. Nagel, L. Musila, M. Muthoni, M. Nikolich, J. L. Nakavuma, M. R. Clokie, *Curr. Opin. Virol.* **2022**, *53*, 101208.
- [19] V. Daubie, H. Chalhoub, B. Blasdel, H. Dahma, M. Merabishvili, T. Glonti, N. De Vos, J. Quintens, J.-P. Pirnay, M. Hallin, O. Vandenberg, *Front. Cell. Infect. Microbiol.* **2022**, *12*, 1000721.
- [20] N. Ács, M. Gambino, L. Brøndsted, *Front. Microbiol.* **2020**, *11*, 594868.
- [21] K. Dąbrowska, *Med. Res. Rev.* **2019**, *39*, 2000.
- [22] J.-P. Pirnay, G. Verbeken, P.-J. Ceysens, I. Huys, D. De Vos, C. Ameloot, A. Fauconnier, *Viruses* **2018**, *10*, 64.
- [23] D. Štveráková, O. Šedo, M. Benešík, Z. Zdráhal, J. Doškař, R. Pantůček, *Viruses* **2018**, *10*, 176.
- [24] Y. Tian, C. Xue, W. Zhang, C. Chen, L. Ma, Q. Niu, L. Wu, X. Yan, *Anal. Chem.* **2022**, *94*, 14299.
- [25] M. Unterer, M. Khan Mirzaei, L. Deng, *Microbiol. Spectr.* **2023**, *11*, e0514922.
- [26] A. Ashkin, J. M. Dziedzic, *Science* **1987**, *235*, 1517.
- [27] Y. Pang, H. Song, W. Cheng, *Biomed. Opt. Express* **2016**, *7*, 1672.
- [28] K. C. Neuman, E. H. Chadd, G. F. Liou, K. Bergman, S. M. Block, *Biophys. J.* **1999**, *77*, 2856.
- [29] R. P. Badman, F. Ye, M. D. Wang, *Curr. Opin. Chem. Biol.* **2019**, *53*, 158.
- [30] M. Tardif, J.-B. Jager, P. R. Marcoux, K. Uchiyamada, E. Picard, E. Hadji, D. Peyrade, *Appl. Phys. Lett.* **2016**, *109*, 133510.
- [31] P. Kang, P. Schein, X. Serey, D. O'Dell, D. Erickson, *Sci. Rep.* **2015**, *5*, 12087.
- [32] Y.-F. Chen, X. Serey, R. Sarkar, P. Chen, D. Erickson, *Nano Lett.* **2012**, *12*, 1633.
- [33] Y. Shi, Y. Wu, L. K. Chin, Z. Li, J. Liu, M. K. Chen, S. Wang, Y. Zhang, P. Y. Liu, X. Zhou, H. Cai, W. Jin, Y. Yu, R. Yu, W. Huang, P. H. Yap, L. Xiao, W. Ser, T. T. B. Nguyen, Y.-T. Lin, P. C. Wu, J. Liao, F. Wang, C. T. Chan, Y. Kivshar, D. P. Tsai, A. Q. Liu, *Laser Photonics Rev.* **2022**, *16*, 2100197.

- [34] M. Tardif, E. Picard, V. Gaude, J.-B. Jager, D. Peyrade, E. Hadji, P. R. Marcoux, *Small* **2022**, *18*, 2103765.
- [35] J.-P. Pirnay, B. G. Blasdel, L. Bretaudeau, A. Buckling, N. Chanishvili, J. R. Clark, S. Corte-Real, L. Debarbieux, A. Dublanquet, D. De Vos, J. Gabard, M. Garcia, M. Goderdzishvili, A. Górski, J. Hardcastle, I. Huys, E. Kutter, R. Lavigne, M. Merabishvili, E. Olchawa, K. J. Parikka, O. Patey, F. Pouilot, G. Resch, C. Rohde, J. Scheres, M. Skurnik, M. Vanechoutte, L. Van Parys, G. Verbeken, et al., *Pharm. Res.* **2015**, *32*, 2173.
- [36] M. R. Lee, P. M. Fauchet, *Opt. Lett.* **2007**, *32*, 3284.
- [37] N. Descharmes, U. P. Dharanipathy, Z. Diao, M. Tonin, R. Houdré, *Phys. Rev. Lett.* **2013**, *110*, 123601.
- [38] R. Therisod, M. Tardif, P. R. Marcoux, E. Picard, J.-B. Jager, E. Hadji, D. Peyrade, R. Houdré, *Appl. Phys. Lett.* **2018**, *113*, 111101.
- [39] M. Minkov, I. A. D. Williamson, L. C. Andreani, D. Gerace, B. Lou, A. Y. Song, T. W. Hughes, S. Fan, *ACS Photonics* **2020**, *7*, 1729.
- [40] M. L. Juan, R. Gordon, Y. Pang, F. Eftekhari, R. Quidant, *Nat. Phys.* **2009**, *5*, 915.
- [41] L. Neumeier, R. Quidant, D. E. Chang, *New J. Phys.* **2015**, *17*, 123008.
- [42] J. Hu, S. Lin, L. C. Kimerling, K. Crozier, *Phys. Rev. A* **2010**, *82*, 053819.
- [43] N. Descharmes, U. P. Dharanipathy, Z. Diao, M. Tonin, R. Houdré, *Lab Chip* **2013**, *13*, 3268.
- [44] S. Bouguelia, Y. Roupioz, S. Slimani, L. Mondani, M. G. Casabona, C. Durmort, T. Vernet, R. Calemczuk, T. Livache, *Lab Chip* **2013**, *13*, 4024.
- [45] T. van Leest, J. Caro, *Lab Chip* **2013**, *13*, 4358.
- [46] P. Jing, J. Wu, G. W. Liu, E. G. Keeler, S. H. Pun, L. Y. Lin, *Sci. Rep.* **2016**, *6*, 19924.
- [47] K. C. Neuman, S. M. Block, *Rev. Sci. Instrum.* **2004**, *75*, 2787.
- [48] P. Y. Liu, L. K. Chin, W. Ser, T. C. Ayi, P. H. Yap, T. Bourouina, Y. Leprince-Wang, *Lab Chip* **2014**, *14*, 4237.
- [49] K. F. Ross, E. Billing, *J. Gen. Microbiol.* **1957**, *16*, 418.
- [50] G. C. Brittain, Y. Q. Chen, E. Martinez, V. A. Tang, T. M. Renner, M.-A. Langlois, S. Gulnik, *Sci. Rep.* **2019**, *9*, 16039.
- [51] Z. J. Storms, M. R. Teel, K. Mercurio, D. Sauvageau, *PHAGE New Rochelle N* **2020**, *1*, 27.
- [52] P. Perlemoine, P. R. Marcoux, E. Picard, E. Hadji, M. Zelsmann, G. Mugnier, A. Marchet, G. Resch, L. O'Connell, E. Lacot, *PLoS One* **2021**, *16*, e0248917.
- [53] M. Kornienko, N. Kuptsov, R. Gorodnichev, D. Bespiatykh, A. Guliaev, M. Letarova, E. Kulikov, V. Veselovsky, M. Malakhova, A. Letarov, E. Ilina, E. Shitikov, *Sci. Rep.* **2020**, *10*, 18612.
- [54] R. J. Jackman, T. M. Floyd, R. Ghodssi, M. A. Schmidt, K. F. Jensen, *J. Micromech. Microeng.* **2001**, *11*, 263.